New Journal of Physics
The open access journal at the forefront of physics

Deutsche Physikalische Gesellschaft DPG
IOP Institute of Physics

Published in partnership with: Deutsche Physikalische Gesellschaft and the Institute of Physics

OPEN ACCESS

RECEIVED
7 January 2022

REVISED
12 May 2022

ACCEPTED FOR PUBLICATION
30 May 2022

PUBLISHED
20 June 2022

PAPER

Plasma electron acceleration in a non-resonant microwave heating scheme below the electron cyclotron frequency

A Köhn-Seemann[1,*], G Birkenmeier[2,3], P Diez[1], E Holzhauer[1], S Merli[1], M Ramisch[1], G Sichardt[1] and U Stroth[2,3]

[1] Institut für Grenzflächenverfahrenstechnik und Plasmatechnologie, Universität Stuttgart, 70569 Stuttgart, Germany
[2] Max-Planck-Institut für Plasmaphysik, EURATOM Association, Garching, Germany
[3] Physik-Department E28, Technische Universität München, 85747 Garching, Germany
[*] Author to whom any correspondence should be addressed.

E-mail: koehn@igvp.uni-stuttgart.de

Keywords: magnetized plasmas, whistler waves, mode coupling in plasmas, microwave plasma heating, stellarator, electric and magnetic measurements, particle acceleration

Abstract

Microwave heating of over-dense plasmas is routinely achieved in the stellarator TJ-K. In contrast to usually applied heating scenarios in tokamaks or stellarators, an operational regime is described where the heating occurs well below the electron cyclotron frequency but still well above the lower hybrid frequency. Microwave energy is deposited at the so-called O-resonance, accompanied by a small population of high-energy electrons with an energy up to 100 keV. These electrons are responsible for a significant toroidal net current and the occurrence of hard x-rays. Requirements for achieving this heating regime are described together with a novel scheme for plasma-electron acceleration.

1. Introduction

The first experiments in which plasmas were created exclusively by microwaves date back to 1948 [1]. Since then, microwave heating has become an indispensable tool both in high-temperature [2] and in low-temperature plasma physics [3]. In high-temperature plasmas, absorption of the injected microwaves usually occurs where the wave frequency equals the electron cyclotron frequency (ECF) or its harmonics [4, 5]. In low-temperature plasmas, heating at the electron cyclotron resonance frequency is restricted to the fundamental resonance. Alternatively, heating at the upper-hybrid resonance is reported in such plasmas [6–8]. Another possibility to transfer microwave energy to both high and low-temperature plasmas is provided by electron Bernstein waves (EBWs), which are electrostatic waves that need to be coupled to electromagnetic waves at the plasma boundary [9]. The EBW is very well absorbed at the ECF and its harmonics, even in low-temperature plasmas. All of these heating methods have one feature in common: the microwave frequency must be equal to or higher than the ECF. Here, we present a method where the plasma is heated by microwaves whose frequency is *below* the ECF throughout the cross section of the plasma such that heating at the ECF (via EBWs for example) is not possible. This process has first been mentioned in reference [10] and discussed briefly in the context of the ionosphere in the 1960s [11, ch 21.13] and for laboratory experiments a few years later in more detail [12, 13]. Only since a decade ago, it is reported or investigated in the context of fusion-related experiments [14–17]. It provides a very robust and efficient heating method for over-dense plasmas whose densities exceed the cut-off density and where the ECF is above the microwave frequency. We report on the acceleration of electrons to high energies in this heating scenario, resulting in comparably large currents.

Plasmas are known to be capable of generating strong electric fields which can be used to accelerate charged particles to very high energies [18–21]. In our toroidal plasma geometry we found evidence for the acceleration of electrons up to 100 keV without the existence of a toroidal electric field as in tokamaks. In this paper, we describe plasma heating below the ECF in the TJ-K stellarator and propose an acceleration mechanism for the generation of the observed high energy electrons.

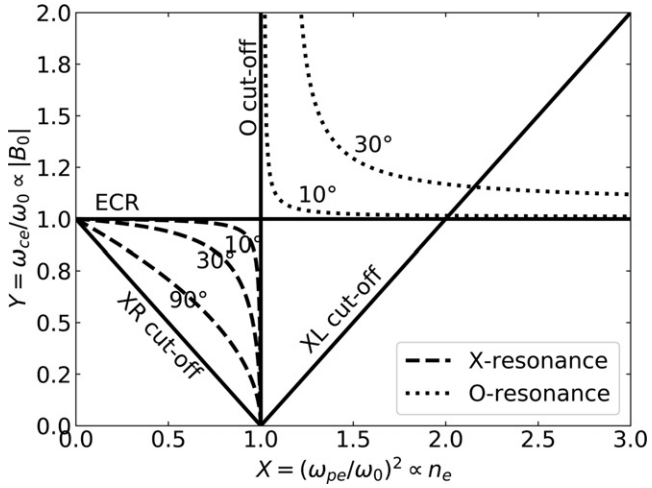

Figure 1. CMA diagram showing the solutions of the dispersion relation for waves in magnetized plasmas for varying angles θ between the wave vector and the background magnetic field.

This paper is organized as follows: the introduction is followed by a brief overview about relevant theoretical aspects on plasma-microwave interaction. The stellarator TJ-K is described in section 3. Experimental results are described and discussed in section 4. Section 5 deals with the mechanism to generate the population of high-energy electrons and a summary in section 6 concludes the paper.

2. Microwaves in a plasma

A variety of text books deal with the interaction between plasma and electromagnetic waves, e.g. references [22, 23]. A significant amount of these texts were written in the 1960s describing mainly ionosphere-related experiments or observations [11, 24]. Their theoretical considerations are partly of great detail and can be applied also in a very general context. Accordingly, the basis for this section is given by these books.

Let's us first assume the case of a plane wave with an angular frequency ω_0 propagating at an angle θ with respect to a background magnetic field $\mathbf{B}_0$, where the wave vector $\mathbf{k}$ is oriented along the z-axis in a Cartesian coordinate system. Introducing $X = \omega_{pe}^2/\omega_0^2$ and $Y = \omega_{ce}/\omega_0$ with ω_{pe} and ω_{ce} the electron plasma and cyclotron frequencies, respectively, and neglecting collisions, the index of refraction N is given by the *Appleton–Hartree equation*:

$$N^2 = 1 - \frac{2X(1-X)}{2(1-X) - Y^2\sin^2\theta \pm \sqrt{Y^4\sin^4\theta + 4Y^2(1-X)^2\cos^2\theta}}. \tag{1}$$

Cut-offs and resonances are found by solving the equation for $N \to 0$ and $N \to \infty$, respectively:

$$\omega_{cut1} = \omega_{pe}, \qquad \omega_{cut2,3} = \pm\omega_{ce}/2 + \sqrt{\omega_{ce}^2/4 + \omega_{pe}^2} \tag{2}$$

$$\omega_{res1,2}^2 = \frac{\omega_{ce}^2 + \omega_{pe}^2}{2} \pm \sqrt{\left(\frac{\omega_{ce}^2 + \omega_{pe}^2}{2}\right)^2 - \omega_{ce}^2\omega_{pe}^2\cos^2\theta}. \tag{3}$$

In this framework, the cut-offs do not depend on the angle θ, in contrast to the resonances.

Figure 1 shows a CMA diagram for various values of θ with the corresponding cut-offs and resonance as labeled in the plot. The well known cases for parallel ($\theta = 0$) and perpendicular ($\theta = \pi/2$) propagation can be found in the diagram: the resonance for the X-mode, the upper-hybrid resonance (dashed line), and its two cut-offs, the R and the L cut-off, the O-mode cut-off, and for parallel propagation the electron cyclotron resonance frequency at $Y = 1$. For oblique propagation, the resonances are modified: with decreasing value of θ the X-resonance curve becomes more concave. Furthermore, in the upper right corner of the diagram a new resonance appears which, according to reference [12, ch 1.4.10], is referred to as *O-resonance*. This resonance offers the possibility to transfer wave energy to a plasma whose ECF exceeds the microwave frequency, i.e. $Y > 1$. For a microwave beam entering the plasmas from the low density region, however, the resonance is shielded by the O-mode cut-off and since it does not extend to low densities, as can be seen from figure 1, no microwave energy can directly be coupled to it.

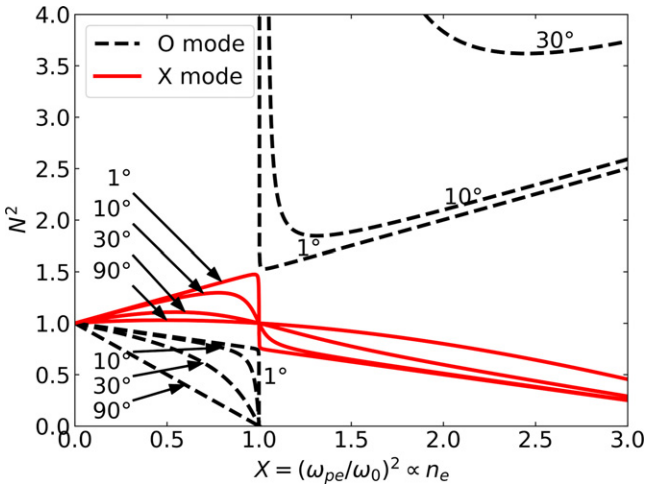

Figure 2. Refractive index as a function of the normalized plasma density X for varying values of θ and a normalized background magnetic field strength of $Y = 3$.

This fact becomes evident when looking at the refractive index shown in figure 2 as a function of X for a background magnetic field corresponding to $Y = 3$ (which is similar to the values used in the experiments described in this work). An O-mode traveling along a density gradient, starting at $X = 0$, first encounters a cut-off before it can reach the O-resonance. With decreasing angle θ, however, the refractive indices for O- and X-mode approach each other quite closely around the O-cut-off ($X = 1$) and the O-resonance. The evanescent layer separating the cut-off and the resonance becomes thinner and tunneling through this layer becomes possible resulting in linear mode conversion. This X–O conversion resembles the well-known O–X conversion for $Y < 1$ where it is the first step in the O–X–B mode conversion process finally resulting in the generation of EBWs. The waves, which are excited in the X–O conversion process, are usually referred to as *Whistler waves* with both $Y > 1$ and $X > 1$. When they approach the O-resonance they become more and more longitudinal, the increasing refractive index leads to an increasing wave electric field and absorption by the plasma becomes relevant. This can be either due to Landau damping [25] or collisional damping. The X–O conversion process is discussed in great detail in reference [13].

3. The TJ-K stellarator

TJ-K is an $l = 1$, $m = 6$ stellarator of type torsatron with major and minor radii of 0.6 and 0.1 m, respectively [26, 27]. The low-temperature plasmas in TJ-K are characterized by electron temperatures of $T_e \approx 10$ eV and plasma densities of $n_e \approx 10^{18}$ m^{-3}. The background magnetic field can be continuously ramped up to a maximum value of $B_0 = 500$ mT. Large port sizes allow for excellent diagnostics access to the plasmas. The dimensionless similarity to fusion edge plasmas [27] and the possibility to use Langmuir probes over the whole cross section account for investigation of plasma dynamics as a key research topic at TJ-K incorporating e.g. zonal flow physics [28, 29], turbulent energy transfer [30, 31], geometry dependence [32], scrape-off layer dynamics [33, 34], amongst others. Being equipped with a number of different microwave heating systems and diagnostics, the other major topic consists in investigations of plasma microwave interactions [6, 15].

3.1. Microwave heating

Two microwave heating systems are used for the experiments presented in this paper. The first consists of a magnetron producing 2.45 GHz microwaves with a maximum output power of 3 kW. A quartz window serves as vacuum transition, and a horn antenna emits the microwaves into the vacuum vessel. The second system is based on a klystron, amplifying microwaves in the frequency range 7.9–8.4 GHz to a maximum power of 3 kW. A window made of high-density polyethylene acts as a vacuum transition, and a phased-array antenna emits the microwaves into the vacuum vessel [35].

3.2. Diagnostics

Radial plasma density and electron temperature profiles are obtained from Langmuir probes [36]. A single-chord heterodyne interferometer operating at 64 GHz is used for measuring the line-averaged density [26] and to calibrate the radial plasma density profiles to absolute densities. The radiative power losses of

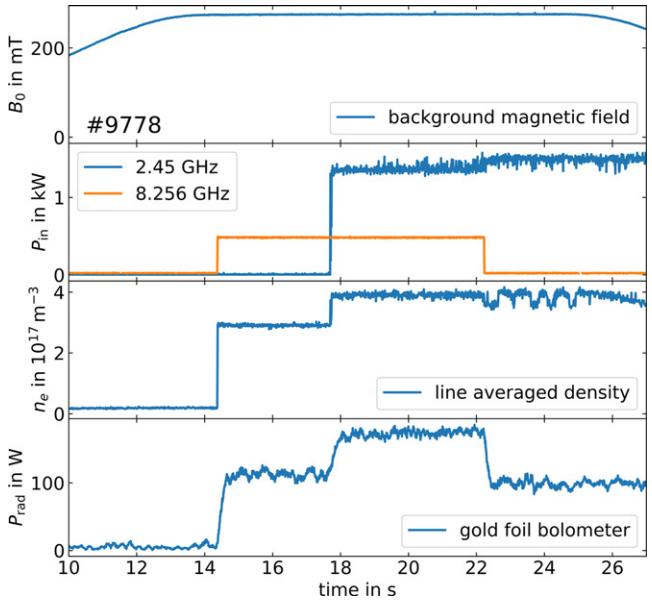

Figure 3. Time traces of a helium discharge ($p_0 \approx 23$ mPa) that was started resonantly with 8.256 GHz and then sustained by non-resonant heating with 2.45 GHz only.

the plasma are deduced from an eight channel bolometer system [37]. Each channel consists of a 1.3×3.8 mm^2 gold foil exposed to plasma radiation. A fine mesh made of stainless steel with a mesh size (lattice constant) of 0.224 mm and a wire size of 0.028 mm shields the bolometer from microwaves.

To measure toroidal net currents, an external Rogowski coil is used [38]. An external diamagnetic loop allows to obtain the plasma energy content. Due to the low values of the toroidal net current and of the plasma energy content, synchronous detection using lock-in amplifiers must be applied which requires periodic modulation of the microwave heating power. This allows to detect net currents down to a few hundred mA and plasma energy contents as low as 10 mJ. The injected microwave power is monitored via directional couplers and microwaves diodes (crystal detector and zero-bias Schottky diodes) installed in the transmission lines.

A semi-conductor detector, namely a Si(Li) diode in reversed biased configuration and shielded from optical light via a beryllium window, is used to measure the x-rays emitted by high-energy electrons. A pulse height analyzer allows to obtain an energy spectrum up to a detection limit of approximately 200 keV. To get absolute values the diagnostic needs to be calibrated. This is done via an energy calibration unit, where a tungsten filament is heated with 3.5 A and biased with 10 kV. A set of different anode materials allows then to perform the calibration. Since this calibration unit is an integral part of the pulse height analyzer itself, a calibration is performed in advance of every shot session (only negligible differences were found between different shot sessions). Details about the diagnostic can be found in reference [39, ch 3.2.6.1]. Finally, a commercial Geiger–Müller counter located outside of the vacuum vessel is used to detect ionizing radiation from energies of 30 keV upwards [40]. This diagnostic is not equipped with a digital or analog output which would allow to synchronize its measurements with scans of the plasma parameters. The pulse-height analyzer is, however, capable of such quantitative studies, see section 5.

4. Experimental results characterizing the non-resonant microwave heating scenario

Non-resonant heating is observed at a high magnetic field strength of $B \approx 250$ mT without an electron cyclotron resonance frequency for 2.45 GHz inside the vacuum vessel. The plasma is initiated with the 8 GHz system which has an electron cyclotron resonance inside the confinement region. Figure 3 shows the plasma breakdown with the 8 GHz heating system. Despite the lack of a cyclotron resonance, additional heating at 2.45 GHz is observed at about 17.7 s. The line-averaged density strongly increases which is due to the fact that the gas in the seed plasma was not fully ionized. When the 8 GHz system is switched off, the plasma density is maintained with the 2.45 GHz at its high level. Experiments have shown that the line-averaged density of the seed plasma has to surpass a minimum value of $\bar{n}_e \approx 7 \cdot 10^{16}$ m^{-3} to allow for non-resonant heating. This density corresponds approximately to the O-mode cut-off density of 2.45 GHz.

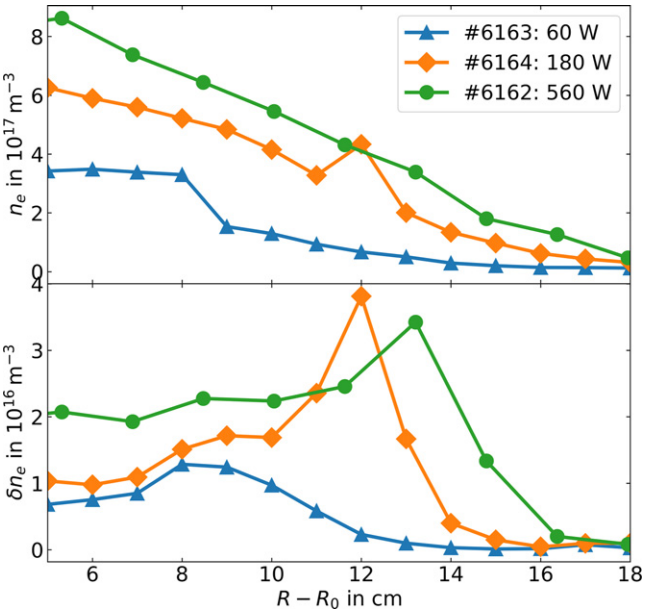

Figure 4. (Top) Radial profiles of the plasma density and (bottom) the induced density modulation amplitude related to the deposition profiles for three shots with varying heating power, both obtained from Langmuir probe measurements performed from the plasma center to the vessel wall (the solid lines are a guide to the eye).

The power deposition profiles were estimated from microwave power modulation experiments: the microwave power acts on the electron temperature and then via ionization on the plasma density. Hence, the radial density perturbation profile reflects the power deposition profile. This technique has been used successfully previously at TJ-K [6] and similar experiments [41, 42]. Particle confinement times τ_n in TJ-K can be estimated from the $1/e$ decay time of the plasma density when switching-off the microwave heating power [43]. Langmuir probes operated in the ion saturation regime were used to obtain values on the order of $\tau_n \approx 1$ ms. The modulation frequency used for estimating the power deposition profiles was $f_{\mathrm{mod}} = 29.7$ kHz and thus on a much faster time scale than typical particle confinement times in TJ-K.

Figure 4 shows the radial density profiles and the induced density modulation amplitude related to the radial deposition profiles for three different discharges with argon as working gas at a neutral gas pressure of $p_0 = 4$ mPa. The heating power has been varied as indicated in the plot. The plasma density increases with increasing heating power, which is due to an increase in the degree of ionization. Assuming the neutral gas to be at room temperature, $T_{\mathrm{gas}} = 293$ K, the neutral gas density before the plasma discharge starts can be calculated with the ideal gas law $n_{\mathrm{gas}} = p_{\mathrm{gas}}/(k_{\mathrm{B}} T_{\mathrm{gas}})$. Assuming further singly ionized particles, the degree of ionization before non-resonant heating is approximately $\alpha_{\mathrm{ion},1} = n_{\mathrm{i}}/n_{\mathrm{gas}} \approx 0.30$, and $\alpha_{\mathrm{ion},2} \approx 0.40$ afterwards for this discharge. In all cases the microwave power is deposited in regions where the density is in the range of $n_{\mathrm{e}} \approx 3 \ldots 4 \times 10^{17}$ m^{-3} which is well above the O-mode cut-off density of 2.45 GHz of $n_{\mathrm{e}} \approx 0.75 \times 10^{17}$ m^{-3}. The power deposition, identified by the peak in the profile of the density variation δn_{e}, is shifted outwards with increasing heating power. The only possible explanation for the observed power deposition seems to be absorption of Whistler waves in the vicinity of the O-resonance as explained in section 2.

A toroidal net current on the order of a few amperes has been previously identified in TJ-K to be driven by EBWs coupled to externally injected microwaves [15]. In the non-resonant heating scheme, considerably higher currents are measured, as shown in figure 5 (left) where the current is shown as a function of the neutral gas pressure. Increasing the neutral gas pressure corresponds to decreasing collision times, i.e. the observed current decreases with increasing collision frequency. A very similar behavior is found for the plasma energy content as obtained from a diamagnetic loop, see figure 5 (right): much higher values are obtained in the non-resonant heating schemes as compared to typical discharges in the standard operational regimes, which yield values of $W_{\mathrm{dia}} \approx 0.2$ J [15]. The signal is also found to decrease with increasing collision frequency. The plasma energy content calculated from plasma density and temperature profiles obtained from Langmuir probe measurements in the non-resonant heating regime, is roughly an order of magnitude lower than the values from the diamagnetic loop. Since the Langmuir probes in TJ-K are only sensitive to the electron temperature of the bulk plasma, whereas the diamagnetic energy (obtained from the diamagnetic loop) includes also the high-energy electron population, the existence of the latter

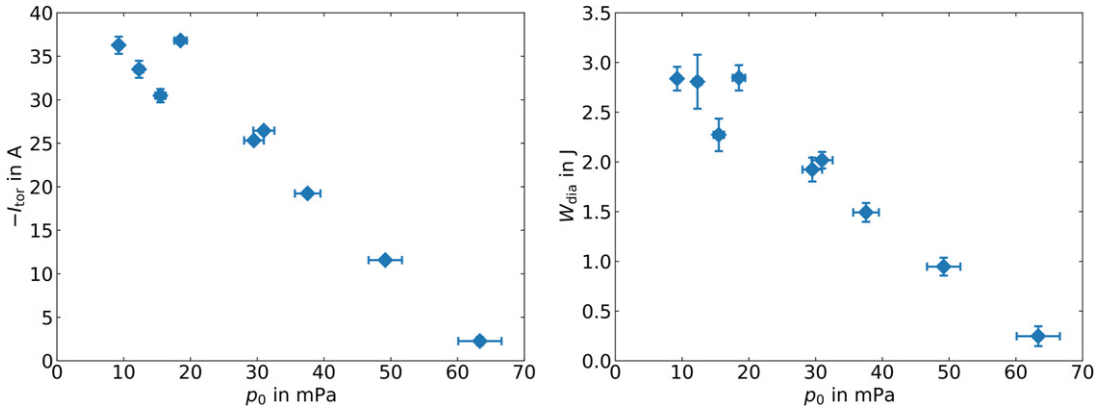

Figure 5. (Left) Toroidal net current as a function of the neutral gas pressure for a series of helium discharges, (right) energy content as obtained from a diamagnetic loop for the same series of discharges. Synchronous detection as explained in section 3.2 required power modulation of 2.45 GHz ($P_{in} = 1.6$ kW), the 8.3 GHz heating sustained a seed plasma during the power-off phase, background magnetic field was $B_0 \approx 270$ mT.

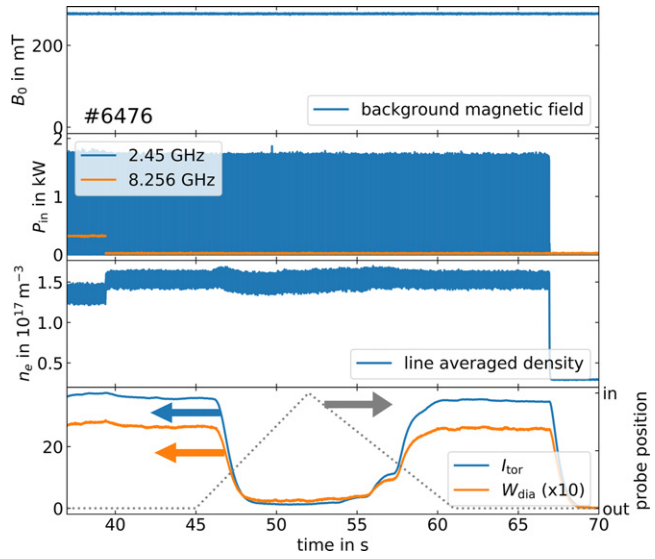

Figure 6. Time traces of a helium discharge ($p_0 \approx 24$ mPa) where the 2.45 GHz was power-modulated to allow detection of the toroidal net current (via the Rogowski coil) and the diamagnetic signal. From $t \approx 46$–60 s, a Langmuir probe was present in the plasma resulting in a strong reduction of the toroidal net current and diamagnetic signal while the line-averaged plasma density hardly changes.

seems to be very likely[4]. Together with the occurrence of the comparably high toroidal current and diamagnetic signals, ionizing radiation was detected with an increase in the count rate at the Geiger–Müller counter (located approximately 1.5 m outside the vacuum vessel) by 2–3 orders of magnitude compared to the background radiation level. Those effects support the hypothesis of the existence of a substantial high-energy, non-thermal electron population.

A Langmuir probe moved into a non-resonantly heated plasma, quenches the toroidal net current and the diamagnetic signal strongly decreases (figure 6). This effect is independent of the bias voltage of the Langmuir probe, i.e. the probe acts here basically as an obstacle stopping the fast electrons by interrupting their trajectories. The plasma density remains unchanged during the probe movement (figure 6). The hot electron density must therefore be significantly below that of the bulk plasma.

In figure 7, the diamagnetic signal is shown as function of the radial position of the Langmuir probe allowing to determine the radial location of the non-thermal electron population: at around $R - R_0 \approx 12$ cm, a strong decrease of the signal is observed roughly corresponding to the radial position

[4] In the standard discharge regimes, the plasma energy content obtained from the diagmagnetic loop and from Langmuir probes have been shown to agree within the error bars [44].

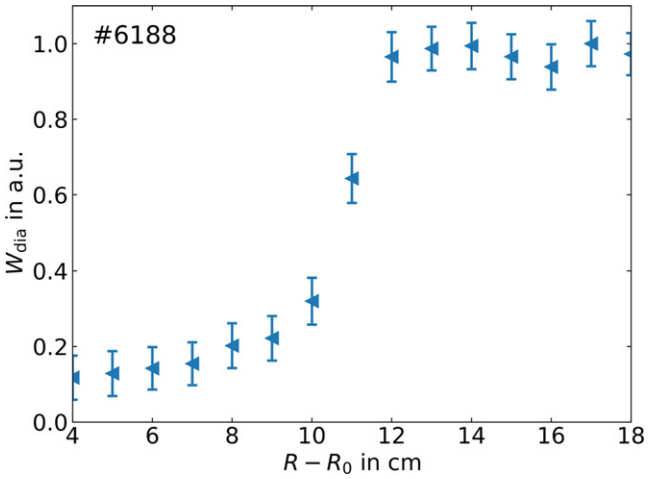

Figure 7. Plasma energy content of a helium discharge ($p_0 \approx 18$ mPa) as obtained from the diamagnetic loop as a function of the position of a radially moving Langmuir probe.

where the power deposition is located (see figure 4). Note that the Rogowski coil reveals a current drop at the same position (see figure 6). The ionizing radiation as measured with the Geiger–Müller counter was also found to drop to background radiation levels when the Langmuir probe reached that position coming from the outboard side. From this we conclude that the fast electrons are generated in the vicinity of the O-resonance, where the microwave becomes increasingly electrostatic. The wavelength becomes shorter when approaching the O-resonance, see figure 2, and strong wave electric fields can be expected which may generate the electrons responsible for the observed toroidal net current, energy content, and the ionizing radiation.

Electrons accelerated *along* the magnetic field lines (co-direction) exhibit drift planes exceeding the radii of the flux surfaces for a starting point on the low-field side. Electrons accelerated *against* the direction of the magnetic field lines (counter-direction) on the other hand are moving on drift planes inside the flux surfaces where they have started on, see e.g. [45, ch 9.2.2]. As explained in the previous paragraph, the acceleration is likely to happen at the plasma boundary. A net current can be generated this way, since co-directed electrons are more likely to intersect with the vessel wall (due to their enlarged drift planes) and thus getting lost as compared to electrons moving in counter-direction. A research project simulating the trajectories of these electrons in the 3D geometry of TJ-K is currently underway in order to confirm the hypothesis of the current generation mechanism.

5. Generation of high-energy electrons

As described in the previous section, a population of fast electrons is generated when non-resonant heating is applied. These electrons must be generated from the bulk electrons whose temperature is approximately $T_e \approx 10$ eV. From the measurement with the diamagnetic loop, see figure 7, the energy of the fast electron population can be estimated to

$$W_{dia}^{fast} \approx 5 \cdot W_{dia}^{bulk}. \tag{4}$$

Furthermore, figure 6 allows to conclude that the density of the fast electron population is small compared to the bulk plasma density, i.e. $n_e^{fast} \leqslant 10^{-2} \cdot n_e^{bulk}$, since the line-averaged density does not change noticeably when the fast electron population is collected by the Langmuir probe. With the diamagnetic energy content being proportional to average density and temperature, $W_{dia} \propto n_e T_e$, and assuming that the high-energy electrons reside in an annulus with a width of 3 cm at the plasma boundary (to be compared with the average minor radius of 10 cm), this allows to estimate a minimum temperature for the hot electrons, $T_e^{fast} \gtrsim 4.5 \times 10^3 \cdot T_e^{bulk}$. Since $T_e^{bulk} \approx 10$ eV, this corresponds to $T_e^{fast} \gtrsim 45$ keV. Note that this estimate of a minimum energy corresponds approximately to the lower detection limit of the Geiger–Müller counter (30 keV).

A maximum electron energy can be estimated from a closer look at the acceleration process itself (similar to the approach used in reference [46]). From figures 6 and 7 we concluded that the fast electron population exists only near the O-resonance where the power deposition occurs. There, only Whistler waves can propagate, as described in section 2. They are guided along the magnetic field lines, see e.g. reference [47], and become increasingly electrostatic when approaching the O-resonance. An acceleration length

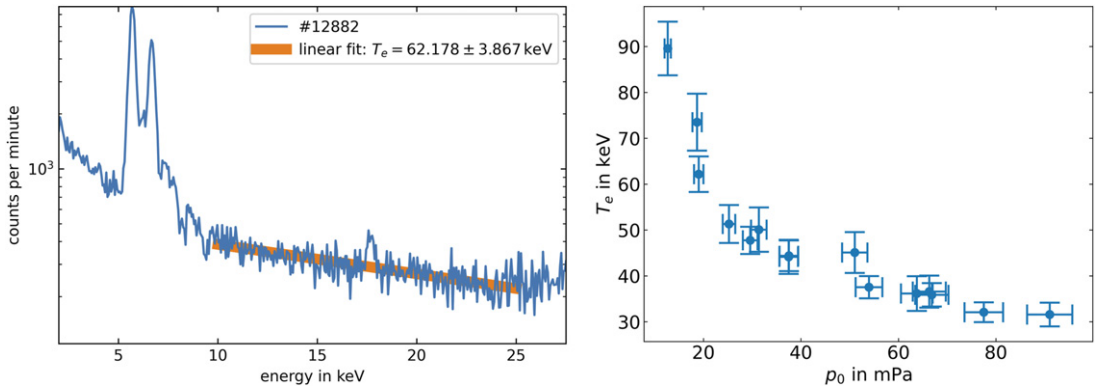

Figure 8. (Left) Soft x-ray spectrum as obtained from the pulse height analyzer, characteristic lines originate from the $KL_{2,3}$ transitions of Cr and the $KL_{2,3}$ transitions of Fe (i.e. from interaction of the high-energy electrons with the stainless steel vacuum vessel), the linear fit (note the semi-logarithmic scale) is performed to the continuous part of the spectrum. (Right) Temperature of the high-energy electrons obtained from fits as indicated in the left figure as a function of neutral gas pressure.

$d_{\mathrm{acc}} \approx 2$ cm parallel to the magnetic field can be estimated from the corresponding refractive index (assuming that the acceleration happens over half a wavelength). We furthermore assume a constant acceleration $a = eE_{\mathrm{acc}}/m_{\mathrm{e}}$, with E_{acc} the accelerating electric field from the microwave, and an acceleration time corresponding to half a wave period, $t_{\mathrm{acc}} = 0.5 \cdot f_0^{-1}$. A maximum acceleration a^{max} is reached when an electron is accelerated a distance d_{acc} for a time period t_{acc}: $a^{\mathrm{max}} = 2d_{\mathrm{acc}}/t_{\mathrm{acc}}^2$. Using this expression for the acceleration, the wave electric field required to achieve a^{max} can be estimated to

$$E_{\mathrm{acc}} = 8 d_{\mathrm{acc}} f_0^2 \frac{m_{\mathrm{e}}}{e}. \tag{5}$$

Inserting the numbers results in a value of $E_{\mathrm{acc}} \approx 6$ MV m^{-1} and a gain in kinetic energy of a single electron of $W_{\mathrm{e}} = E_{\mathrm{acc}} d_{\mathrm{acc}} e \approx 110$ keV. The electron travels therefore with half the speed of light. This high value might be surprising at first but becomes more reasonable when considering that slower, non-relativistic electrons would not be able to escape from the acceleration volume before the wave electric field changes sign and thus cancels out the previous acceleration. The gained energy depends on the acceleration distance as $W_{\mathrm{e}} \propto d_{\mathrm{acc}}^2$ and a small change in the distance would result in a noticeable change in gained energy. As an approximation we will use the value just derived,

$$W_{\mathrm{e}}^{\mathrm{fast}} \lesssim 100 \text{ keV}. \tag{6}$$

To obtain the hot electrons' energy from the pulse height analyzer the diagnostic was calibrated. Figure 8 shows a spectrum obtained in a non-resonantly heated discharge. Two characteristic lines can be seen, attributed to the interaction of the fast electrons with the vacuum vessel. More importantly, a continuous spectrum is present. Due to the exponential decay of the continuum radiation emitted by the high-energy electrons, a linear fit to the semi-logarithmic plot allows to determine their energy [36, ch 5.3.5]. Performing this analysis to a series of shots with varying neutral gas pressure results in figure 8 (right). The temperature of the fast electrons drops with increasing neutral gas pressure. Furthermore, the measured temperature values agree with our previous estimations, equation (6).

From the measured toroidal net current strength of $I_{\mathrm{p}} \approx 30$ A (figure 6), the number density of fast electrons $n_{\mathrm{e}}^{\mathrm{fast}}$ can be deduced,

$$I_{\mathrm{p}} = A^{\mathrm{fast}} n_{\mathrm{e}}^{\mathrm{fast}} v^{\mathrm{fast}} e, \tag{7}$$

with A^{fast} the area across which the current flows. According to figure 7, A^{fast} can be roughly described by an annulus with a width of 3 cm. Using the minimum and maximum values for $T_{\mathrm{e}}^{\mathrm{fast}}$, the density of the fast electron population can thus be estimated to

$$n_{\mathrm{e}}^{\mathrm{fast}} \approx 1 \ldots 3 \times 10^{14} \text{ m}^{-3} \tag{8}$$

using the values obtained from helium discharges at $p_0 = 10$ mPa. The density of the fast electrons has, as argued above, a small value compared to the thermal electron density.

Assuming stationary conditions allows to approximate the power coupled to the fast electrons P^{fast} from the losses through collisions,

$$P^{\mathrm{fast}} = \frac{W_{\mathrm{e}} \cdot N_{\mathrm{e}}^{\mathrm{fast}}}{\tau_{\mathrm{sd}}}, \tag{9}$$

where τ_{sd} is the slowing-down time. Due to the relatively low ionization degree in the relevant discharges ($\alpha_{ion} \approx 0.05$ for helium as working gas), the slowing down process of the electrons is dominated by collisions with neutrals as is described by the Bethe Bloch formula for light charged particles. This formula can be applied to estimate the mean rate of energy loss, the *stopping power*, and thus also the distance it takes for an electron to be slowed down (also referred to as *stopping length*) [48]. Tabulated values for helium and argon [49] applied to the parameters of the discharges discussed here, result in stopping lengths on the order of 10^3 km ($\tau_{sd} \approx 10$ ms) for 100 keV electrons and 10 km ($\tau_{sd} \approx 0.5$ ms) for 10 keV electrons. Finally, the minimum power necessary to sustain the population of high-energy electrons can be approximated via equation (9) to be on the order of 10 W for 100 keV electrons and 50 W for 10 keV electrons. Given that the injected microwave power is usually on the order of 1 kW in the respective discharges, these are very reasonable numbers.

6. Summary & conclusion

A novel microwave heating regime in the fusion-related experiment TJ-K has been successfully demonstrated. It consists in heating at frequencies below the ECF but still above the lower hybrid resonance frequency, hence the name *non-resonant heating*. Theoretical considerations and experimental observations allow to draw the conclusion that the power deposition happens at the O-resonance in the over-dense plasma region. Microwave power needs to be coupled to Whistler waves via a tunneling and mode-conversion process in the vicinity of the O-mode cut-off layer. Although the coupling depends in principle on the injection angle of the microwave, this dependence does not play a role here due to the multiple reflections of the injected microwave between the cut-off and the vacuum vessel wall, such that eventually the correct angle is hit (an effect which we refer to as the *Kasparek*-effect, named after our colleague Dr. W Kasparek). A minimum seed plasma density on the order of the O-mode cut-off density was accordingly found to be a requirement for this heating scenario.

Strong wave electric fields at the resonance are proposed to generate high-energy electrons. This population of fast electrons not only results in comparably large toroidal net currents and high diamagnetic signals, it can also lead to significant ionizing radiation when colliding with in-vessel components. Inserting a probe that stops the fast electrons or increasing the neutral gas pressure and thus decreasing the electron mean free path can quench those three effects to levels common for typical operational regimes in TJ-K. Quantitative calculations of the driven toroidal net current being a result of the difference of the drift planes into and against the toroidal magnetic field direction for these fast electrons are currently underway.

For the generation of the high-energy electrons, a new plasma-based acceleration mechanism is proposed which relies on strong electric fields in the vicinity of the O-resonance layer. The acceleration occurs in a narrow volume. Estimations of the electrons' energy derived from this model agree with measurements performed with a pulse height analyzer. By increasing the heating power and optimizing the profiles and discharge conditions, it is conceivable that even higher energies may be reached.

This heating regime has proven to be very robust yielding high plasma densities with only moderate microwave power. It might prove useful for devices flexible enough in their operational space (background magnetic field and microwave heating frequency) to increase substantially their accessible plasma parameters.

Acknowledgments

Valuable discussions with Drs Heinrich Laqua, Torsten Stange, Joachim Stroth, and experimental support by Dr Hendrik Höhnle are gratefully acknowledged by the authors. Torsten Stange deserves a special *thank you* for providing the x-ray diagnostics, whose measurements are an essential part of this work. The authors are also indebted to the efforts of the open-source software community.

Data availability statement

The data that support the findings of this study are available upon reasonable request from the authors.

ORCID iDs

A Köhn-Seemann https://orcid.org/0000-0002-1192-2057
G Birkenmeier https://orcid.org/0000-0001-7508-3646
M Ramisch https://orcid.org/0000-0002-5316-3853
U Stroth https://orcid.org/0000-0003-1104-2233

References

[1] Herlin M A and Brown S C 1948 *Phys. Rev.* **74** 291
[2] Thumm M 2003 *Plasma Phys. Control. Fusion* **45** A143
[3] Moisan M and Pelletier J 1992 *Microwave Excited Plasmas* (Amsterdam: Elsevier)
[4] Bornatici M, Cano R, De Barbieri O and Engelmann F 1983 *Nucl. Fusion* **23** 1153
[5] Erckmann V and Gasparino U 1994 *Plasma Phys. Control. Fusion* **36** 1869
[6] Köhn A, Birkenmeier G, Holzhauer E, Ramisch M and Stroth U 2010 *Plasma Phys. Control. Fusion* **52** 035003
[7] Podestà M, Fasoli A, Labit B, McGrath M, Müller S H, Poli F M and Poli F M 2005 *Plasma Phys. Control. Fusion* **47** 1989
[8] Rypdal K, Fredriksen Å, Olsen O M and Hellblom K G 1997 *Phys. Plasmas* **4** 1468
[9] Laqua H P 2007 *Plasma Phys. Control. Fusion* **49** R1
[10] Poeverlein H 1950 *Z. Phys.* **2** 152
[11] Budden K G 1961 *Radio Waves in the Ionosphere* (Cambridge: Cambridge University Press)
[12] Heald M A and Wharton C B 1965 *Plasma Diagnostics with Microwaves* (New York: Wiley)
[13] Golant V E and Piliya A D 1972 *Sov. Phys. - Usp.* **14** 413
[14] Köhn A, Birkenmeier G, Diez P, Holzhauer E, Ramisch M and Stroth U 2009 *36th EPS Conf. Plasma Phys. ECA* vol 33E
[15] Köhn A *et al* 2013 *Plasma Phys. Control. Fusion* **55** 014010
[16] Kobayashi S *et al* 2011 *Nucl. Fusion* **51** 062002
[17] Otte M, Laqua H P, Marsen S, Podoba Y, Preinhaelter J, Stange T, Urban J, Wagner F and Zhang D 2010 *Contrib. Plasma Phys.* **50** 785
[18] Tajima T and Dawson J M 1979 *Phys. Rev. Lett.* **43** 267
[19] Chen P *et al* 1985 *Phys. Rev. Lett.* **54** 693
[20] Leemans W P *et al* 2014 *Phys. Rev. Lett.* **113** 245002
[21] Adli E *et al* 2018 *Nature* **561** 363
[22] Stix T H 1992 *Waves in Plasmas* (New York: AIP)
[23] Swanson D G 1989 *Plasma Waves* (New York: Academic)
[24] Ginzburg V L 1961 *Propagation of Electromagnetic Waves in Plasma* (New York: Gordon and Breach)
[25] Dawson J 1961 *Phys. Fluids* **4** 869
[26] Krause N *et al* 2002 *Rev. Sci. Instrum.* **73** 3474
[27] Stroth U, Greiner F, Lechte C, Mahdizadeh N, Rahbarnia K and Ramisch M 2004 *Phys. Plasmas* **11** 2558
[28] Manz P, Ramisch M and Stroth U 2009 *Phys. Rev. Lett.* **103** 165004
[29] Birkenmeier G, Ramisch M, Schmid B and Stroth U 2013 *Phys. Rev. Lett.* **110** 145004
[30] Manz P, Birkenmeier G, Ramisch M and Stroth U 2012 *Phys. Plasmas* **19** 082318
[31] Schmid B *et al* 2017 *Phys. Rev. Lett.* **118** 055001
[32] Birkenmeier G, Ramisch M, Fuchert G, Köhn A, Nold B and Stroth U 2013 *Plasma Phys. Control. Fusion* **55** 015003
[33] Fuchert G, Birkenmeier G, Nold B, Ramisch M and Stroth U 2013 *Plasma Phys. Control. Fusion* **55** 125002
[34] Garland S, Fuchert G, Ramisch M and Hirth T 2016 *Plasma Phys. Control. Fusion* **58** 044012
[35] Köhn A *et al* 2008 *AIP Conf. Proc.* **993** 43
[36] Hutchinson I H 2002 *Principles of Plasma Diagnostics* 2nd edn (Cambridge: Cambridge University Press)
[37] Tumanski S 1991 *Rev. Sci. Instrum.* **62** 744
[38] Tumanski S 2007 *Meas. Sci. Technol.* **18** R31
[39] Stange T 2013 *PhD Thesis: Microwave Heating and Diagnostics of Suprathermal Electrons in an Overdense Stellarator Plasma* Technische Universität Berlin
[40] Gamma-Scout GmbH & Co. KG 2009 https://gamma-scout.com
[41] Podoba Y Y *et al* 2007 *Phys. Rev. Lett.* **98** 255003
[42] Ikeda R *et al* 2008 *Phys. Plasmas* **15** 072505
[43] Birkenmeier G 2008 *Diploma Thesis* University of Stuttgart
[44] Merli S 2010 *Diploma Thesis* University of Stuttgart
[45] Stroth U 2005 Transport toroidal plasmas *Plasma Physics: Confinement, Transport and Collective Effects* ed A Dinklage *et al* ch 9 (Berlin: Springer)
[46] Laqua H P, Chlechowitz E, Otte M and Stange T 2014 *Plasma Phys. Control. Fusion* **56** 075022
[47] Pfannmöller J P, Lechte C, Grulke O and Klinger T 2012 *Phys. Plasmas* **19** 102113
[48] Tanabashi M *et al* 2018 *Phys. Rev.* D **98** 030001
[49] Berger M J *et al* 2017 *NIST Standard Reference Database 124* (Last Update to Data content: July 2017; NISTIR 4999)